

## Winding up Dynamics for Matched and Unmatched Elastic Constants in Chiral Nematic Liquid Crystals

E. K. Omori and R. F. de Souza

*Departamento de Física, Universidade Estadual de Maringá, Avenida Colombo*

R. T. de Souza and R. S. Zola

*Departamento de Física, Universidade Estadual de Maringá, Avenida Colombo and*

*Departamento Acadêmico de Física, Universidade Tecnológica Federal do Paraná,*

*Campus Apucarana, Rua Marcílio Dias, 635 CEP 86812-460 – Apucarana, Paraná, Brazil*

### I. ILLUSTRATION OF THE SYSTEM UNDER CONSIDERATION

Figure S1 illustrates the system under consideration in this work. Starting from the Grandjean texture (which is the typical equilibrium structure for a cholesteric confined between two flat substrates with planar anchoring conditions), we apply an electric field until the helix is completely unwound and the Homeotropic structure is achieved. Then, the field is suddenly turned off, and we study the transient states that arise from the time  $t = 0$  ms (considered from the moment the field is shut off) for all the different materials and alignment conditions leading to the return of the Grandjean texture (which takes  $t_r$  ms). The duration of this relaxation process ( $t_r$ ) can vary based on the specific attributes of the sample.

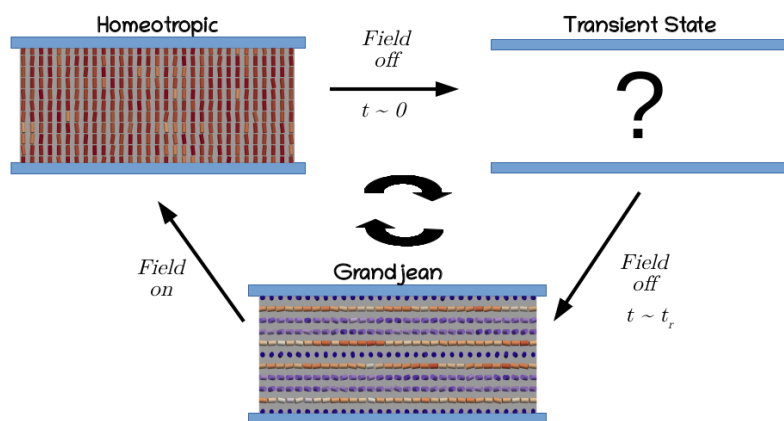


FIG. S1: Illustration of the system under consideration in this work. The sample is initially in the Grandjean state when an electric field is applied and the helical structure unwound. Then, the field is turned off at  $t = 0$  ms and we monitor the transient states leading to the return of the Grandjean structure at time  $t = t_r$ .

### II. LANDAU-DE GENNES MODEL

The Landau-de Gennes free energy is formulated through the symmetric, traceless order parameter tensor  $Q_{ij}$ , integrating all parameters of nematic liquid crystals in the following manner:

$$Q_{ij} = 3/2S(n_i n_j - 1/2\delta_{i,j}) + 1/2P(l_i l_j - m_i m_j) \quad (S1)$$

In this context, ( $S$ ) and ( $P$ ) represent the uniaxial and biaxial order parameters. Here,  $\vec{n}$  denotes the primary director,  $\vec{l}$  signifies the secondary director, and the vector  $\vec{m}$  is defined as  $\vec{n} \times \vec{l}$ . Deviations from the equilibrium values for all

these parameters are interconnected through a free energy density expressed as:

$$\begin{aligned}
f_{LDG}(\mathbf{Q}) = & \frac{a}{2}(T - T^*)\text{Tr}(\mathbf{Q}^2) + \frac{B}{3}\text{Tr}(\mathbf{Q}^3) + \frac{C}{4}\text{Tr}(\mathbf{Q}^2)^2 + \frac{1}{2}L_1(Q_{jk,i})(Q_{jk,i}) \\
& + \frac{1}{2}L_2(Q_{ji,i})(Q_{jk,k}) + \frac{1}{2}L_3Q_{ij}(Q_{kl,i})(Q_{kl,j}) + \frac{1}{2}L_s(Q_{ij,k})(Q_{ik,j}) \\
& + \frac{4\pi}{P_0}L_q\epsilon_{ikl}Q_{ij}(Q_{lj,k}),
\end{aligned} \tag{S2}$$

where  $Q_{ij,k} = \partial Q_{ij}/\partial x_k$  represents the spatial derivative of  $Q_{ij}$  along the  $k$ -th direction, with  $T$  signifying the sample liquid crystal temperature and  $T^*$  the hypothetical temperature for the nematic-isotropic phase transition. In this equation, the initial three terms denote the energy linked to the uniaxial and biaxial order parameters at temperature  $T$ . Meanwhile, the subsequent five terms describe a structure similar to Franks' elastic free energy for the Q-tensor. Here, the variations in the liquid crystal directors  $n$ ,  $l$ , and  $m$  are interconnected with the values of the order parameters  $S$  and  $P$  and their spatial variations.

The nematic order parameter  $S$  in terms of the material parameters  $a$ ,  $B$ , and  $C$  can be found by minimizing eq. S2 as  $S_{eq} = [-B + \sqrt{B^2 - 24AC}]/(6C)$ , with  $A = a(T - T^*)$ . Given  $S_{eq}$  as previously established, and using the approximation  $Q_{ij} = S_{eq}(3/2n_in_j - 1/2\delta_{i,j})$ , one can infer the connection between the elastic parameters of Landau-de Gennes and Frank:[1, 2]:

$$\begin{aligned}
L_1 &= \frac{2(-K_{11} + 3K_{22} + K_{33})}{27S_{eq}^2}; \\
L_2 &= \frac{4(K_{11} - K_{22} - K_{24})}{9S_{eq}^2}; \\
L_3 &= \frac{4(-K_{11} + K_{33})}{27S_{eq}^3}; \\
L_q &= \frac{4K_{22}q_0}{9S_{eq}^2}; \\
L_s &= \frac{4K_{24}}{9S_{eq}^2}.
\end{aligned} \tag{S3}$$

$q_0 = 2\pi/p_0$  represents the chiral wavevector, and  $K_{11}$ ,  $K_{22}$ ,  $K_{33}$  and  $K_{24}$  represent the elastic constants of splay, twist, bend, and saddle-splay, respectively.

To replicate the interaction between the sample and the surfaces, a corresponding form of the Rapini-Papoular anchoring energy was employed for the Q-tensor to produce both the rubbed planar and homeotropic cases:

$$f_{surf} = \frac{1}{2}W(Q_{ij} - Q_{ij}^0)(Q_{ij} - Q_{ij}^0), \tag{S4}$$

where  $W$  denotes the anchoring strength and  $Q_{ij}^0$  represents the optimal Q-tensor value on the surface, defined as  $Q_{ij}^0 = S_{eq}(3/2n_i^0n_j^0 - \delta_{i,j}/5)$ , where  $\vec{n}^0$  is the easy axis of the surface. In addition to modifying molecular orientation, this potential can adjust the parameter  $S$  near the surface. The planar degenerate case was treated here using the Fournier-Galatola energy: [3]

$$f_{surf}(\mathbf{Q}) = W_P \left( \tilde{Q}_{ij}(\mathbf{Q}) - \tilde{Q}_{ij}^\perp(\mathbf{Q}) \right)^2, \tag{S5}$$

where  $W_P$  is the anchoring strength,  $\tilde{Q}_{ij}(\mathbf{Q}) = Q_{ij} + S/3\delta_{ij}$  and  $\tilde{Q}_{ij}^\perp(\mathbf{Q}) = (\delta_{ik} - \nu_i\nu_k)Q_{kl}(\delta_{lj} - \nu_l\nu_j)$ .

Regarding the interaction between the sample and an applied electric field, the energy density is expressed as:

$$f_{ele} = -\frac{1}{3}\Delta\epsilon\epsilon_0(E_iE_jQ_{ij}), \tag{S6}$$

with  $\epsilon_0$  and  $\Delta\epsilon = \epsilon_{\parallel} - \epsilon_{\perp}$  being the vacuum permittivity and the dielectric anisotropy, respectively. Thus, the total free energy of the system can be described by:

$$F_{tot} = \int_{vol} f_{bulk}dV + \oint_{surf} f_{surf}dS, \tag{S7}$$

with  $f_{bulk} = (f_{LdG} + f_{ele})$ . The dynamics of the system can be determined via the Landau-de Gennes dynamical equation, which outlines the progression of  $Q_{ij}$  in the bulk for systems without material flow:

$$\mu_b \frac{dQ_{ij}}{dt} = \Lambda_{ijkl} \left( \frac{\partial f_{bulk}}{\partial Q_{kl}} - \frac{\partial}{\partial x_m} \frac{\partial f_{bulk}}{\partial Q_{kl,m}} \right). \quad (S8)$$

In this context,  $\mu_b = \gamma_b / S_{eq}^2$ , where  $\gamma_b$  denotes the bulk rotational viscosity, accounts for the bulk dissipation. The expression  $\lambda_{ijkl} = \sum_{k=1}^3 \sum_{l=1}^3 (\delta_{i,k} \delta_{j,l} + \delta_{i,l} \delta_{j,k} - 2/3 \delta_{i,j} \delta_{k,l})$  ensures that the tensor  $Q_{ij}$  remains symmetric and traceless. On the surface, the  $Q$  tensor evolves as follows:

$$\mu_s \frac{dQ_{ij}}{dt} = \Lambda_{ijkl} \left( \nu_m \frac{\partial f_{bulk}}{\partial Q_{kl,m}} - \frac{\partial f_{surf}}{\partial Q_{kl}} \right), \quad (S9)$$

where  $\nu_m$  is the  $m$ 's component of the vector normal to the surface, and  $\mu_s$  represents the surface viscosity as previously discussed.

### III. SIMULATION ASPECTS

Our numerical model was constructed using the Comsol framework, offering approximation functions  $\phi_n^e(\mathbf{x})$ , quadrature techniques for spatial integration, a solver for nonlinear equations, and a BDF method for time integration. The full weak form was algebraically processed with Mathematica software, and readers can request the entire expression if needed. More details can be found in reference [4]. To ensure the ratio  $K_{33}/K_{22} = 2$ , the simulation was performed using a set of elastic parameters similar to the MLC6608 host, that is,  $K_{11} = 16.7$  pN,  $K_{22} = 9.05$  pN, and  $K_{33} = 18.1$  pN, which were converted into parameters  $L_i$  by Eq. S3. For the  $K_{33}/K_{22} = 1$  case we used  $K_{11} = 16.7$  pN,  $K_{22} = 18.15$  pN and  $K_{33} = 18.1$  pN. For the  $K_{33}/K_{22} = 0.067$  case, we used  $K_{11} = 12.0$  pN,  $K_{22} = 6.0$  pN and  $K_{33} = 0.4$  pN, which are similar to the values found for the dimer CB7CB [5]. Furthermore, we used  $L_s = 0.0$  pN, and  $q_0 = 2.51 \times 10^{-7}$  m<sup>-1</sup>. For bulk and surface viscosities ( $\gamma_b$  and  $\gamma_s$ ) we used 0.186 Pa<sup>-1</sup> and 10<sup>-8</sup> Pa<sup>-1</sup>, as discussed in the reference [6].

The interaction between the LC and the surfaces was evaluated utilizing the Rapini-Papoular-like anchoring energy, given by Eq. S4, with an anchoring strength of 0.01 Jm<sup>-2</sup>, which represents a strong anchoring situation [7]. Both simulated surfaces were constructed with the easy axis in the  $x$ -direction with a pretilt of 1°; that is, the easy axis can be described by  $\vec{n}^0 = \cos 1^\circ \hat{i} + \sin 1^\circ \hat{k}$ . Using a pretilt can prevent the formation of surface defects, but in the chiral case, the pretilt also creates a preference for the system to have an even or odd number of twists.

To achieve the homeotropic state, a powerful electric field of  $E = 8.14 \times 10^7$  Vm<sup>-1</sup>  $\hat{k}$  was applied for a duration of 1 ms. This field strength is four times greater than the critical electric field required for the planar-to-homeotropic and fingerprint-to-homeotropic transitions in a material characterized by the specified elastic constants and dielectric anisotropy of  $\Delta_e = 4.2$ . The simulations used a mesh of tetrahedral elements with a maximum edge length of 36  $\mu$ m and employed linear interpolation. The system was computed with a variable-order BDF integrator regarding temporal evolution. The simulations progressed over a time frame ranging from milliseconds to several seconds to ensure that the system achieved equilibrium. The system's state was recorded logarithmically, yielding more states at the beginning and fewer as time progressed.

### IV. ELASTIC ENERGY CURVES

We interpolate the mesh for every state during the time evolution to get the directors and calculated Frank's total elastic energy and the individual energies of Splay, Twist, and Bend during the relaxation process. Figs. S2 (a) to (i) show how the normalized elastic energies of Splay, Twist, and Bend, respectively, evolve with log(t) for the cases  $K_{33}/K_{22} = 2$  ((a) to (c)),  $K_{33}/K_{22} = 1$  ((d) to (f)), and  $K_{33}/K_{22} = 0.067$  ((g) to (i)) for all anchoring types studied here. Normalization is done by dividing the energy at any given time by the energy of the homogeneous state after the transition ends, so it is easy to compare the magnitude of the variation during the transition.

### V. SIMULATIONS OF OPTICAL TEXTURES

Optical textures were built by simulating a polarized light microscopy experiment. The optical devices are represented by the Stokes vector and the Mueller matrices [8, 9].

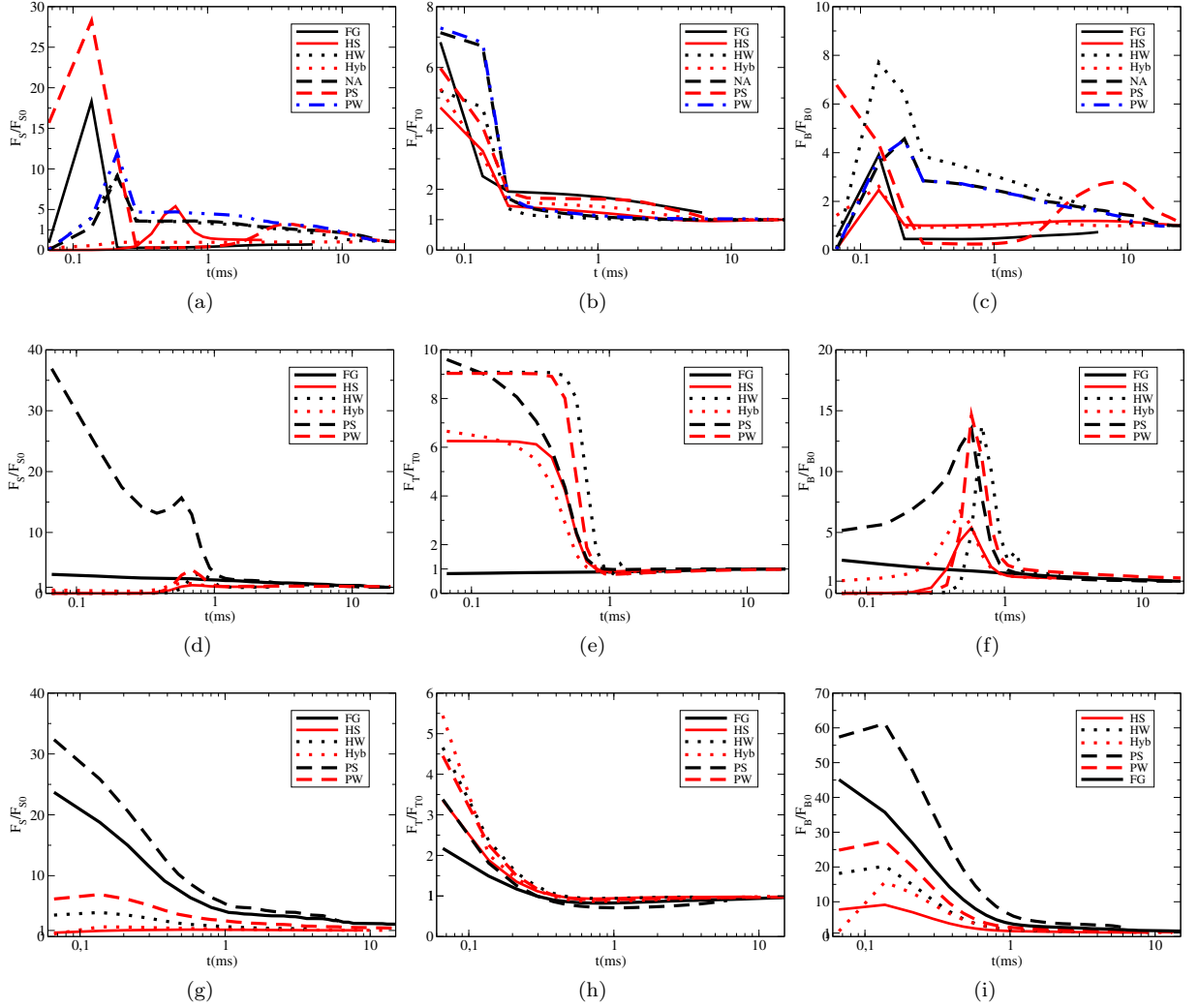


FIG. S2: Dynamics of the three main kinds of energy distortions representing all the cells studied in this work. The first row represents the case  $K_{33} = 2.0K_{22}$ , the second row represents  $K_{33} = 1.0K_{22}$ , and the last row is for  $K_{33} = 0.067K_{22}$ . The columns represent the change in time of Splay, Twist, and Bend deformations. All the energies are normalized by the energy in the final state, after the cell has reached a stable state.

An unpolarized light beam is represented by a Stokes vector as:

$$\vec{T}_{in} = \begin{bmatrix} 1 \\ 0 \\ 0 \\ 0 \end{bmatrix}. \quad (\text{S10})$$

A linear polarizer with polarization angle  $\psi$  with respect to a supposed  $x$  direction in the laboratory frame can be expressed as:

$$P_L(\psi) = \begin{bmatrix} 1 & \cos(2\psi) & \sin(2\psi) & 0 \\ \cos(2\psi) & \cos^2(2\psi) & \cos(2\psi)\sin(2\psi) & 0 \\ \sin(2\psi) & \cos(2\psi)\sin(2\psi) & \sin^2(2\psi) & 0 \\ 0 & 0 & 0 & 0 \end{bmatrix}. \quad (\text{S11})$$

When a polarized light beam emerges in an electric anisotropy medium, such as an LC sample, the dielectric

anisotropy causes a retardation in a component of the beam. The interaction of the beam with the liquid crystals can be written in terms of a Mueller matrix as follows:

$$M_k = \begin{bmatrix} 1 & 0 & 0 & 0 \\ 0 & \cos^2(2\theta) + \sin^2(2\theta) \cos \delta & \sin(2\theta) \cos(2\theta)(1 - \cos \delta) & \sin(2\theta) \sin \delta \\ 0 & \sin(2\theta) \cos(2\theta)(1 - \cos \delta) & \sin^2(2\theta) + \cos^2(2\theta) \cos \delta & -\cos(2\theta) \sin \delta \\ 0 & -\sin(2\theta) \sin \delta & \cos(2\theta) \sin \delta & \cos \delta \end{bmatrix}, \quad (\text{S12})$$

with  $\theta$  being the projection of  $\vec{n}$  in the plane perpendicular to the beam light. The parameter  $\delta$  is given by:

$$\delta = \frac{2\pi h}{\lambda_e} n_o \left( \frac{n_e}{n_{e,k}} - 1 \right), \quad (\text{S13})$$

in which  $h$  is the distance traveled by the beam and  $\lambda_e$  is its wave-length. The parameters  $n_o$  and  $n_e$  are the ordinary and extraordinary refractive indices, respectively. And, finally,  $n_{e,k} = \sqrt{n_o^2 + (n_e^2 - n_o^2) \cos^2 \phi}$ , where  $\phi$  is the angle between  $\vec{n}$  and the beam. A single pixel at a point  $(x, y)$  of the sample is built by considering an unpolarized beam light in the  $z$  direction of the laboratory frame, interacting with a polarizer ( $P_{pol}$ ), all sample sites of the discretized lattice across the  $z$  direction ( $M^{(x,y)}$ ) and finally an analyzer ( $P_{an}$ ). Such a process is mathematically described by the following:

$$\vec{T}_{out}^{(x,y)} = P_{an} \prod_k M_k^{(x,y)} P_{pol} \vec{T}_{in}. \quad (\text{S14})$$

Hence, the intensity of the light transmitted with wavelength  $\lambda$  is given by the first element of  $\vec{T}_{out}$ . Different wavelengths can be combined to build a colorful texture. In this paper, we used nine values of  $\lambda$  (380 nm, 410 nm, 440 nm, 470 nm, 500 nm, 530 nm, 575 nm, 620 nm, 650 nm). Moreover,  $n_o = 1.5$  and  $n_e = 1.7$  respectively, and the length of layer separation of  $h = 0.56 \mu\text{m}$ .

## VI. RELAXATION VIDEOS

As supplementary information, we added 16 videos to illustrate the relaxation dynamics reported in this article. The videos are provided in *.mp4* format. The videos are as follows.

- fg1k2.mp4:** Dynamics of the cell for  $K_{33} = 1.0K_{22}$  and FG anchoring condition.
- fg2k2.mp4:** Dynamics of the cell for  $K_{33} = 2.0K_{22}$  and FG anchoring condition.
- fgbt.mp4:** Dynamics of the cell for  $K_{33} = 0.067K_{22}$  and FG anchoring condition.
- hs1k2.mp4:** Dynamics of the cell for  $K_{33} = 1.0K_{22}$  and HS anchoring condition.
- hs2k2.mp4:** Dynamics of the cell for  $K_{33} = 2.0K_{22}$  and HS anchoring condition.
- hsbt.mp4:** Dynamics of the cell for  $K_{33} = 0.067K_{22}$  and HS anchoring condition.
- hybs1k2.mp4:** Dynamics of the cell for  $K_{33} = 1.0K_{22}$  and Hyb anchoring condition.
- hybs2k2.mp4:** Dynamics of the cell for  $K_{33} = 2.0K_{22}$  and Hyb anchoring condition.
- hybsbt.mp4:** Dynamics of the cell for  $K_{33} = 0.067K_{22}$  and Hyb anchoring condition.
- na2k2.mp4:** Dynamics of the cell for  $K_{33} = 2.0K_{22}$  with free boundaries.
- ps1k2.mp4:** Dynamics of the cell for  $K_{33} = 1.0K_{22}$  and PS anchoring condition.
- ps2k2.mp4:** Dynamics of the cell for  $K_{33} = 2.0K_{22}$  and PS anchoring condition.
- psbt.mp4:** Dynamics of the cell for  $K_{33} = 0.067K_{22}$  and PS anchoring condition.
- pw1k2.mp4:** Dynamics of the cell for  $K_{33} = 1.0K_{22}$  and PW anchoring condition.
- pw2k2.mp4:** Dynamics of the cell for  $K_{33} = 2.0K_{22}$  and PW anchoring condition.
- pwbt.mp4:** Dynamics of the cell for  $K_{33} = 0.067K_{22}$  and PW anchoring condition.

---

[1] H. Mori, E. C. Gartland, J. R. Kelly, and P. J. Bos, Japanese Journal of Applied Physics **38**, 135 (1999), URL <https://doi.org/10.1143/jjap.38.135>.

- [2] E. Willman, F. A. Fernandez, R. James, and S. E. Day, *IEEE Transactions on Electron Devices* **54**, 2630 (2007).
- [3] J.-B. Fournier and P. Galatola, *Europhysics Letters* **72**, 403 (2005), URL <https://dx.doi.org/10.1209/epl/i2005-10253-5>.
- [4] E. K. Omori, R. F. de Souza, A. Jakli, R. T. de Souza, and R. S. Zola, *Phys. Rev. E* **106**, 064701 (2022), URL <https://link.aps.org/doi/10.1103/PhysRevE.106.064701>.
- [5] C.-J. Yun, M. R. Vengatesan, J. K. Vij, and J.-K. Song, *Applied Physics Letters* **106**, 173102 (2015), ISSN 0003-6951, [https://pubs.aip.org/aip/apl/article-pdf/doi/10.1063/1.4919065/14315092/173102\\_1\\_online.pdf](https://pubs.aip.org/aip/apl/article-pdf/doi/10.1063/1.4919065/14315092/173102_1_online.pdf), URL <https://doi.org/10.1063/1.4919065>.
- [6] R. de Souza, D.-K. Yang, E. Lenzi, L. Evangelista, and R. Zola, *Annals of Physics* **346**, 14 (2014), ISSN 0003-4916, URL <https://www.sciencedirect.com/science/article/pii/S0003491614000694>.
- [7] D. Yang and S. Wu, *Fundamentals of Liquid Crystal Devices*, Wiley Series in Display Technology (Wiley, 2014), ISBN 9781118752005, URL <https://books.google.com.br/books?id=W53mBQAAQBAJ>.
- [8] F. Xu, H. S. Kitzerow, and P. P. Crooker, *Phys. Rev. A* **46**, 6535 (1992).
- [9] E. Berggren, C. Zannoni, C. Chiccoli, P. Pasini, and F. Semeria, *Phys. Rev. E* **50**, 2929 (1994).